Supplementary Materials

Probing and modeling cell-cell communication in 2D biomimetic tissues

C. Vincent[1], S. Ravindran[1,2], A. M. Prevost[1], L.-L. Pontani[1], O. Bénichou[3] and E. Wandersman[1*]

[1] *Laboratoire Jean Perrin, CNRS UMR 8237, Sorbonne Université, 4 place Jussieu, 75005 Paris, France*
[2] *Laboratoire Matière et Systèmes Complexes, CNRS UMR 7057, Université Paris Cité, 10 Rue Alice Domon et Léonie Duquet, 75013 Paris, France*
[3] *Laboratoire de Physique Théorique de la Matière Condensée, CNRS UMR 7600, Sorbonne Université, 4 place Jussieu, 75005 Paris, France*

Image Analysis

Once the images are acquired, image processing is necessary in order to make them usable for analysis. The main objective of this step is to fill the possible "holes" between the droplets present in the network (Fig. S1), since these could potentially be detected as droplets, thus introducing errors in the analysis. The first image of the sequence is therefore opened in ImageJ. On this image, a mask is manually applied and the pixel intensity is replaced by a null intensity. In the experiments, it sometimes happens that slight evaporation is observed ($\frac{\Delta R}{R} < 10\%$), which induces a compaction of the network over time and therefore a movement of the droplets. When the network moves significantly, the mask is redone on several images of the sequence in order to adjust it. Once this step is completed, the images are ready to be analyzed with Matlab.

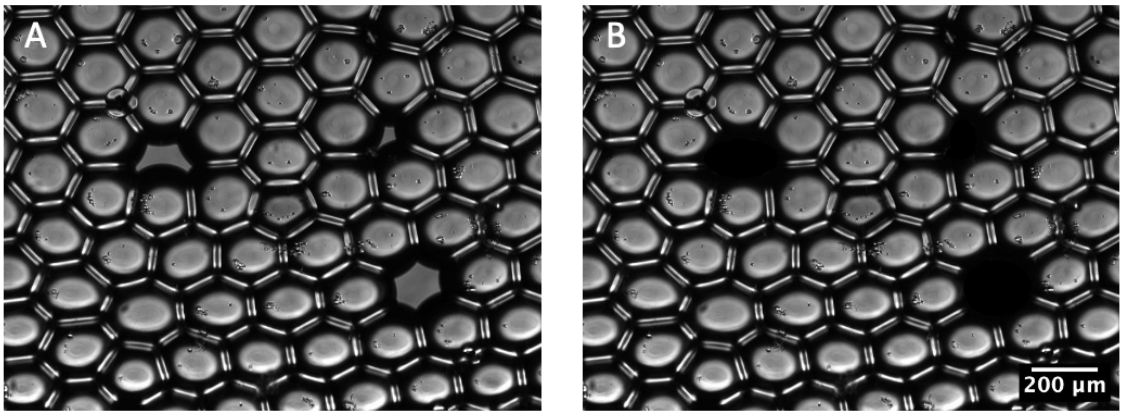

Figure S1: *Images of the droplet network in bright field. (A) Before processing (B) After processing, after applying a mask to fill the holes.*

Bright-field images are used to study the topology of the network, defined by the way the droplets are connected to each other. Fluorescence imaging enables quantification of Calcein diffusion from the fluorescent source droplet into neighboring droplets when the membrane contains nanopores.

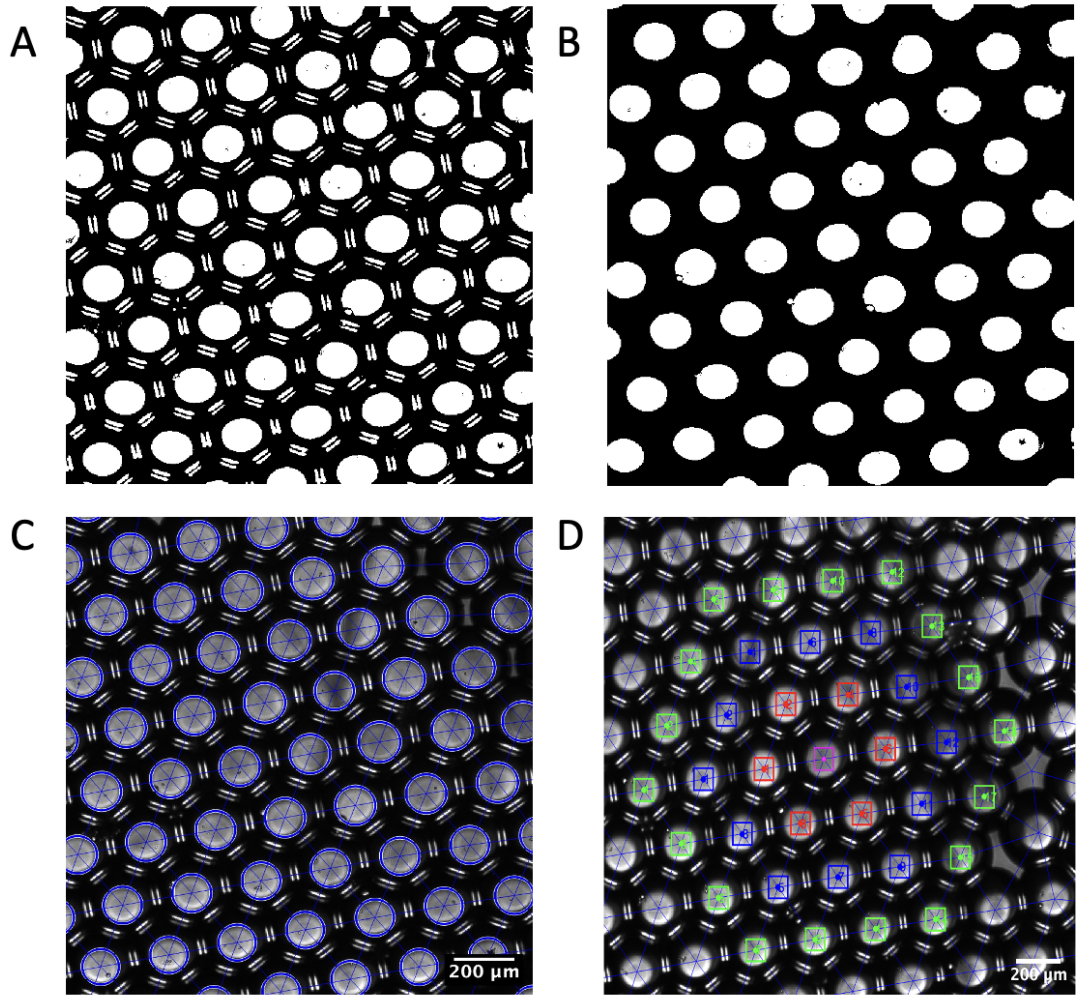

Figure S2: *Image analysis (A) Binarized image. (B) After processing with the Matlab regionprops function. (C) Overlaid with the Delaunay triangulation (blue lines), which reveals how the droplets are connected. (D) A droplet network in bright field, in which the source at the center (magenta square), the first (red), second (blue), and third (green) neighbors are identified by squares overlaid on the image.*

The first step of the analysis consists in detecting the droplets (Fig. S2). To do so, the image is first binarized in order to clearly identify the different regions, then the Matlab *regionprops* function is applied to extract the positions of the droplet centers.
Next, we seek to identify how these centers are connected to each other using a Delaunay triangulation. The Delaunay triangulation method is used to determine the connection links between points in a set [**?**]. In the case of the analysis of the droplet network, this method allows to identify the neighborhood relationships between droplets from the positions of the centers extracted from the binarized images. Once the triangulation is performed, a mesh of the links between each droplet and its neighbors is obtained. It is then possible, thanks to this mesh, to construct the adjacency matrix A_{ij} of the network, giving the connections between the different droplets. In practice, A_{ij} equals 1 if droplets i and j are in physical contact, and 0 otherwise.

By classifying the droplets according to their rank of neighborhood with respect to a given fluorescent source, it then becomes possible to analyze the diffusion of fluorophores in the network.

To identify the fluorescent source, the average intensity is calculated in each droplet within the analysis area (colored squares in Figure S2D). The source is the one with the maximum intensity. Thanks to the adjacency matrix obtained with the Delaunay triangulation, it is then possible to determine the neighborhood rank of each droplet relative to the source.

At each time, the average intensities are measured for the first, second, and third neighbors of the source, as well as in the source itself.
In Figure S3, the intensities in each droplet are plotted as a function of time to quantify the diffusion from the source through the network.

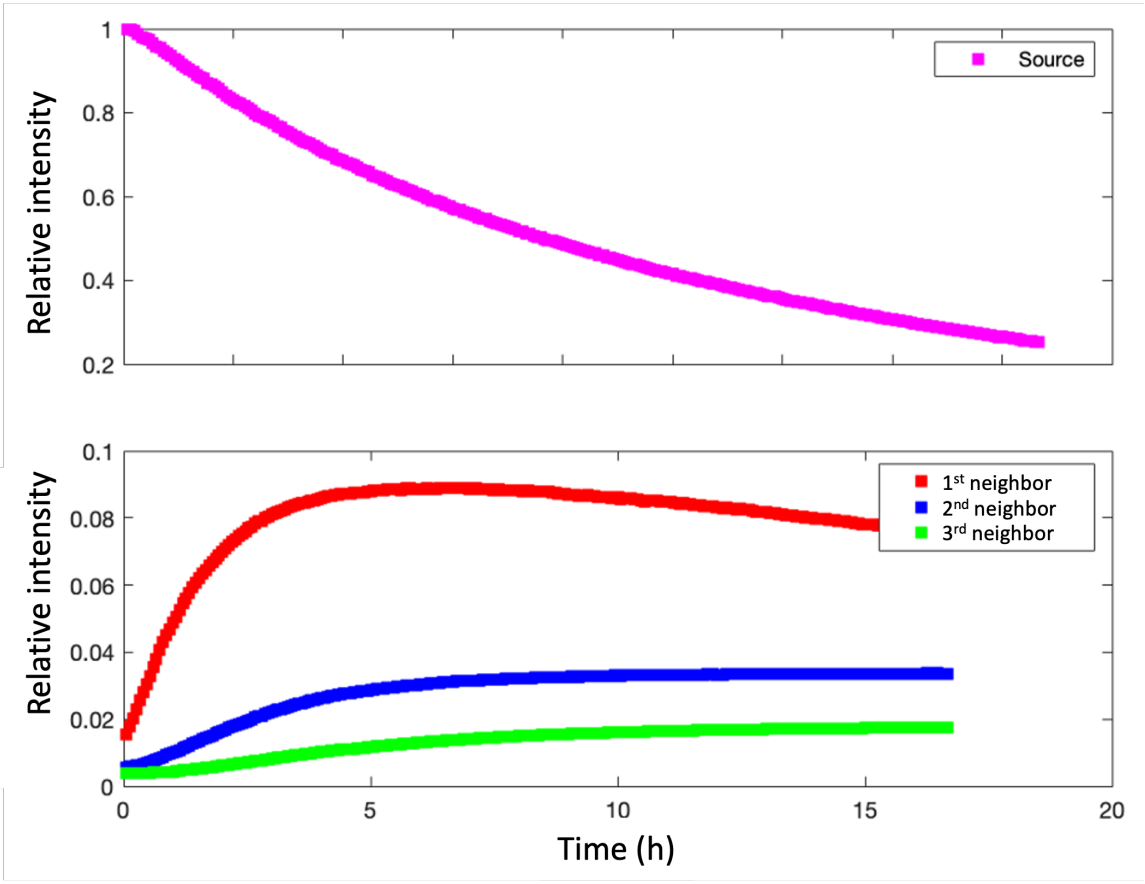

Figure S3: *Example of the curves obtained after image analysis. These curves show the relative fluorescence intensity averaged over the droplets of each neighborhood rank as a function of time. This plot corresponds to a nanopore concentration of 100 $\mu g/mL$. The magenta curve represents fluorescence decay in the source droplet; the red, blue, and green curves correspond to diffusion in the first, second, and third neighbors, respectively.*

For the source droplet, its intensity at each time point is normalized by its maximum intensity which corresponds to its intensity at the beginning of the experiment, at $t = 0$: $I_{Norm}(l_s, t) = \frac{I(l_s,t)}{I(l_s,t=0)}$.

The normalization of the intensity for the droplets neighboring the source is given by:

$$p(l_i, t) = I_{Norm}(l_i, t) = \frac{I(l_i, t) - I_{bk}}{I(l_s, t = 0)}$$

with l_s, the position of the source droplet and l_i, the position of the droplet of interest.

Each droplet acts as a small lens, and thus the attenuated image of the source can be seen in the first, second, and third neighbors. To correct for this, we take $I_{bk} = I(l_i, t = 0)$ for the second and third neighbors.
The case of the first neighbors is slightly different, since diffusion has sometimes already begun in certain first neighbors when the imaging of the network starts. Moreover, we observed that it is sometimes also anisotropic. As a consequence, for the first neighbors we chose $I_{bk} = \min(I(l_i, t = 0))$. Normalizing the intensities by I_{bk} therefore allows us to solve the problem of the reflection of the source in the other neighbors.

We also examined how the intensity curves were modified by changing the analysis area on the droplets, i.e., the region over which the intensity is averaged. Still with the aim of counteracting the effect of the source reflection on its neighbors, the analysis area, reduced in size, is tilted by 30 degrees and shifted so as not to be located in the source reflect. However, the effect of the source reflection is marginal on the distribution of the times of interest, since the intensity curves obtained after changing the area are not significantly different.

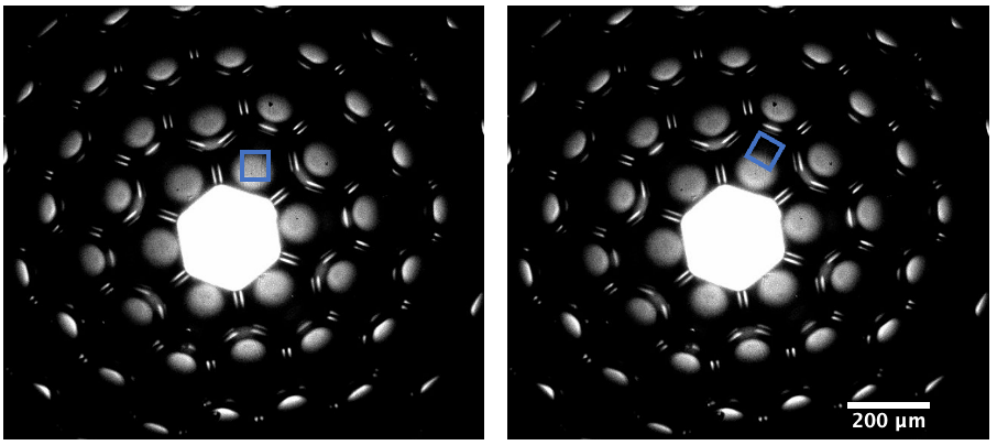

Figure S4: *Modification of the analysis area represented by a blue square. The initial area considered is shown on the left. The area after rotation and once shifted corresponds to the image on the right. The contrast was enhanced to illustrate the lens effect produced by the source on the neighboring droplets.*

Theoretical model

We aim to construct a theoretical model corresponding to the physical model governing the diffusion of calcein molecules through the pores in a two-dimensional droplet network. The goal is to find the presence probability that the fluorophore is located at a given site at time t. In practice, the fluorescent molecules must diffuse to the pore, so the waiting time is random. The distribution of these waiting times for passing from one cell to another can be modeled by an exponential distribution $g(t) = \lambda e^{-\lambda t}$. A given Calcein molecule waits for a random time before moving to the next droplet. This random waiting time qualitatively corresponds to the time needed for the molecule to reach a nanopore in the membrane (see discussion section in the main text). The displacement of the fluorophore at time t does not depend on its previous displacement, hence the process under study is memoryless, i.e., Markovian. We chose an exponential distribution because such a distribution is the only one that corresponds to a memoryless process.

We will first develop the general case, then consider the case of the square lattice, and finally present the case of the model on a hexagonal lattice, which corresponds most closely to our experimental configuration (Fig. 2 in the main text).

Probability distribution for a general geometry

Discrete case

We are interested in the probability $P_n(\vec{l}|\vec{0})$ that a walker is at position $\vec{l}$ in dimension d at time n, given that it started from position $\vec{0}$ at time 0. At time $n+1$, this probability depends on all the possible positions it occupied at time n and can be written as:

$$P_{n+1}(\vec{l}|\vec{0}) = \sum_{l'} P_n(\vec{l'}|\vec{0}) p(\vec{l} - \vec{l'}) \tag{1}$$

where the $\vec{l'}$ are the possible positions at time n, and $p(\vec{l}-\vec{l'})$ is the probability of making a jump from $\vec{l'}$ to $\vec{l}$. This recurrence relation is a convolution of the form: $h(l) = \int dl' f(l')g(l-l')$. Since the Fourier transform of a convolution of two functions is the product of the Fourier transforms of the functions, we can therefore write in Fourier space:

$$\tilde{h}(\vec{k}) = \tilde{f}(\vec{k}) \times \tilde{g}(\vec{k}) \tag{2}$$

Equation 1 can thus be rewritten:

$$\tilde{P}_{n+1}(\vec{k}) = \tilde{P}_n(\vec{k}) \times \Lambda(\vec{k}) \tag{3}$$

In this equation, $\Lambda(\vec{k})$, called the structure factor, is a function that defines the nature of the network under study and of the random walk:

$$\Lambda(\vec{k}) = \sum_{l} p(l) e^{-i\vec{k}\cdot\vec{l}} \tag{4}$$

By recurrence, it is easy to show that:

$$\tilde{P}_n(\vec{k}) = [\Lambda(\vec{k})]^n \times \tilde{P}_0(\vec{k}) \tag{5}$$

Since $P_0(\vec{l}) = \delta(\vec{l} - \vec{0})$ (a probability of 1 of being at position 0), Equation 4 becomes:

$$\tilde{P}_n(\vec{k}) = [\Lambda(\vec{k})]^n \tag{6}$$

$P_n(l)$ is obtained from the inverse Fourier transform of $\tilde{P}_n(\vec{k})$:

$$P_n(l) = \int \frac{d^d k}{(2\pi)^d} e^{-i\vec{k}\cdot\vec{l}} [\Lambda(\vec{k})]^n \tag{7}$$

Applying the discrete Laplace transform, $P(l,\xi) = \sum_{n=0}^{\infty} P_n(l), \xi^n$ with $\xi = e^{-s}$, and substituting into Equation 6 gives:

$$P(l,\xi) = \int \frac{d^d k}{(2\pi)^d} e^{-i\vec{k}\cdot\vec{l}} \sum_{n=0}^{\infty} [\Lambda(\vec{k})\xi]^n \tag{8}$$

The sum in Equation 8 can be simplified, as it corresponds to a geometric series. For $\xi\Lambda < 1$, it can be written as:

$$\sum_{n=0}^{\infty} [\Lambda(\vec{k})\xi]^n = \frac{1}{1-\xi\Lambda} \tag{9}$$

Equation 8, after substituting the summation term, becomes:

$$\boxed{P(l,\xi) = \int \frac{d^d k}{(2\pi)^d} e^{-i\ \vec{k}\cdot\vec{l}} \frac{1}{1-\xi\Lambda}} \tag{10}$$

Using the fact that $\frac{1}{A} = \int_0^\infty dt, e^{-At}$, applied to Equation 10, we obtain:

$$P(\vec{l},\xi) = \int \frac{d^d k}{(2\pi)^d} \int_0^\infty dt e^{-i\vec{k}\cdot\vec{l}} e^{-t(1-\xi\Lambda)} \tag{11}$$

Continuous case

Up to this point in the model, the time steps considered were discrete. We now consider that the time between successive jumps is also a random variable with probability density $\Psi(t)$. In our model, an exponential waiting-time density $\Psi(t) = \lambda e^{-\lambda t}$ is chosen. Its Laplace transform is denoted $\tilde{\Psi}(s)$. The occupancy probability $p(l,t)$ in this continuous-time case can be related to the occupancy probability in the discrete-time case $P(l,t)$ by means of the Montroll–Weiss theorem [**?**].

Montroll-Weiss theorem: If $P(l,\xi) = \sum_{n=0}^{\infty} P_n(l), \xi^n$ is the generating function of the site occupancy probability for a discrete-time walk on a lattice, then the Laplace transform of $p(l,t)$, the probability density of being at l at time t in the continuous case, is given by:

$$\hat{p}(\vec{l},s) = \frac{1-\hat{\Psi}(s)}{s} P(\vec{l},\hat{\Psi}(s))$$

Substituting ξ into Equation 9 gives:

$$P(\vec{l},\hat{\Psi}(s)) = \int \frac{d^d k}{(2\pi)^d} e^{-i\ \vec{k}\cdot\vec{l}} \frac{1}{1-\hat{\Psi}(s)\Lambda} \tag{12}$$

Applying the Montroll–Weiss theorem:

$$\hat{p}(\vec{l},s) = \frac{1-\hat{\Psi}(s)}{s} \int \frac{d^d k}{(2\pi)^d} e^{-i\ \vec{k}\cdot\vec{l}} \frac{1}{1-\hat{\Psi}(s)\Lambda} \tag{13}$$

An exponential waiting-time density is considered:

$$\Psi(t) = \lambda e^{-\lambda t} \tag{14}$$

where λ is a characteristic waiting rate (unrelated to Λ, the structure factor).

$$\hat{\Psi}(s) = \int_0^\infty \lambda e^{-(\lambda+s)t}\ dt \tag{15}$$

$$\hat{\Psi}(s) = \frac{\lambda}{\lambda+s} \tag{16}$$

This yields $\frac{1-\hat{\Psi}}{s} = \frac{1}{\lambda+s}$
Thus, by taking the inverse Laplace transform of Equation 9:

$$p(\vec{l},t) = \frac{1}{4\pi^2} \int_0^\infty \frac{ds\ e^{st}}{\lambda+s} \int \frac{e^{i\ \vec{k}\cdot\vec{l}}}{1-\frac{\lambda}{\lambda+s}\Lambda} d^2k \tag{17}$$

$$= \frac{1}{4\pi^2} \int_0^\infty ds\ e^{st} \int \frac{d^2k\ e^{i\ \vec{k}\cdot\vec{l}}}{\lambda+s-\lambda\Lambda} \tag{18}$$

$$p(\vec{l},t) = \frac{1}{4\pi^2}\int_0^\infty ds\ e^{st}\int \frac{d^2k\ e^{i\ \vec{k}\cdot\vec{l}}}{\lambda(1-\Lambda)+s} \tag{19}$$

The integral over s in the previous equation takes the form:

$$\int \frac{ds\ e^{st}A(\vec{k})}{B(\vec{k})+s}$$

with $A(\vec{k}) = e^{i\ \vec{k}\cdot\vec{l}}$ and $B(k) = \lambda(1-\Lambda(\vec{k}))$, and which can be rewritten as:

$$\frac{A(\vec{k})}{B(\vec{k})}\int \frac{ds\ e^{st}B(\vec{k})}{B(\vec{k})+s} = \frac{A(\vec{k})}{B(\vec{k})}B(\vec{k})\ e^{-B(\vec{k})t} = A(\vec{k})\ e^{-B(\vec{k})t}$$

Equation 19 can be rewritten as:

$$\boxed{p(\vec{l},t) = \frac{1}{4\pi^2}\int_0^\infty ds\ e^{st}\int d^2k\ e^{i\ \vec{k}\cdot\vec{l}}\ e^{-(\lambda(1-\Lambda(\vec{k}))t)}} \tag{20}$$

This general equation provides the occupancy probability for any network topology, given its structure factor Λ.

Continuous-time random walk on a square lattice

In a 2D square lattice, we have:
$\Lambda(k_1,k_2) = \frac{1}{2}(cos(k_1)+cos(k_2))$

With this structure factor, we obtain:

$$p(\vec{l},t) = \frac{e^{-\lambda t}}{4\pi^2}\int_{-\pi}^{+\pi}\int_{-\pi}^{+\pi} dk_1dk_2\ cos(k_1l_1+k_2l_2)\ e^{-\lambda t(\frac{cos(k_1)+cos(k_2)}{2})} \tag{21}$$

As the cosine function is even:

$$p((l_1,l_2),t) = \frac{1}{\pi^2}e^{-\lambda t}\int_0^{+\pi}\int_0^{+\pi} dk_1dk_2\ cos(k_1l_1+k_2l_2)\ e^{-\lambda t(\frac{cos(k_1)+cos(k_2)}{2})} \tag{22}$$

For a square lattice, the general case gives :

$$\boxed{p((l_1,l_2),t) = e^{-\lambda t}\ I_{l_1}\left(\frac{\lambda t}{2}\right)\ I_{l_2}\left(\frac{\lambda t}{2}\right)} \tag{23}$$

with I Bessel functions.

Model on a hexagonal lattice

In a 2D hexagonal lattice, a site l has six possible jump choices (Fig. S5), leading to:
$\Lambda(k_1,k_2) = \frac{1}{6}(2cos(k_1)+2cos(k_2)+2cos(k_1+k_2))$
$\Lambda(k_1,k_2) = \frac{1}{3}(cos(k_1)+cos(k_2)+cos(k_1+k_2))$

In the same way as for the square lattice model, we obtain for the hexagonal lattice:

$$\boxed{p((l_1,l_2),t) = \frac{e^{-\lambda t}}{4\pi^2}\int_{-\pi}^{+\pi}\int_{-\pi}^{+\pi} dk_1dk_2\ cos(k_1l_1+k_2l_2)\ e^{-\lambda t(\frac{cos(k_1)+cos(k_2)+cos(k_1+k_2)}{3})}} \tag{24}$$

In contrast to the square lattice case, this equation does not admit an analytical solution but can be solved numerically.

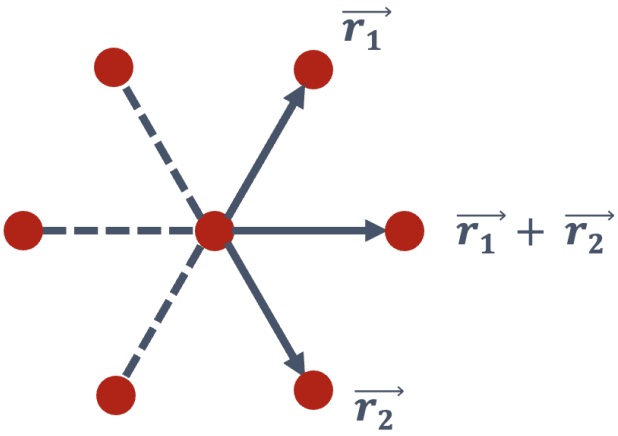

Figure S5: *Diagram illustrating the six possible jumps from a site l in a hexagonal lattice.*

Validation with numerical simulations

To validate the square and hexagonal models, we compared the theoretical predictions obtained in each case with numerical simulations.
To this end, we simulated in Matlab a continuous-time random walk with exponentially distributed waiting times on 2D square and hexagonal lattices. A random walker is started at the origin of the lattice at $t = 0$, and a random time is generated from an exponential distribution. Then, a new position is chosen among the neighboring sites, and this experiment is repeated 50,000 times. For a given site (for example $l = (1, 0)$), we then evaluate the proportion of these realizations leading to this position at a given time. These simulations are also valid for an arbitrary lattice.
In this way, we can compare the presence probability curves obtained from the simulations with the analytical predictions for the square lattice.

Presence probability curves are plotted as a function of time for different coordinates, varying the neighborhood degree, using the analytical predictions of Equation 23. These curves are then compared with those obtained from simulations of a continuous-time random walk with exponential waiting times on a 2D square lattice (Fig. S6). Analytical predictions and simulations are in excellent agreement, within numerical uncertainties. However, for the same neighborhood degree, the probabilities differ depending on the coordinates. For example, for second neighbors, the probability is not the same at (0,2) and (1,1). These droplets are not topologically equivalent: at (0,2) the site is connected to only one first neighbor (at (0,1)), whereas at (1,1) the site is connected to two first neighbors (at (1,0) and (0,1)). This qualitatively explains why the probability is higher for a droplet at (1,1) (two precursors) than at (0,2) (one precursor) at same times. The occupancy probability is also plotted for the hexagonal model.

Equation 24 does not admit an analytical solution; instead, we plot a numerically obtained solution for the presence probability and compare it with simulations of a continuous-time random walk with exponential waiting times on a 2D hexagonal lattice (Fig. S7). Here too, the agreement between numerical results and simulations is excellent, supporting the validity of our theoretical approach.

As in the square lattice model, the presence probability is higher for a droplet with two precursors than for one with only a single precursor. For the hexagonal model, the numerical solution of the theoretical equation matches the simulation results well.

In both square and hexagonal lattices, the theoretical models are in very good agreement with their corresponding numerical simulations. In our experiments, the compacted droplet network is more consistent with a hexagonal lattice than with a square lattice (Fig. 2 in the

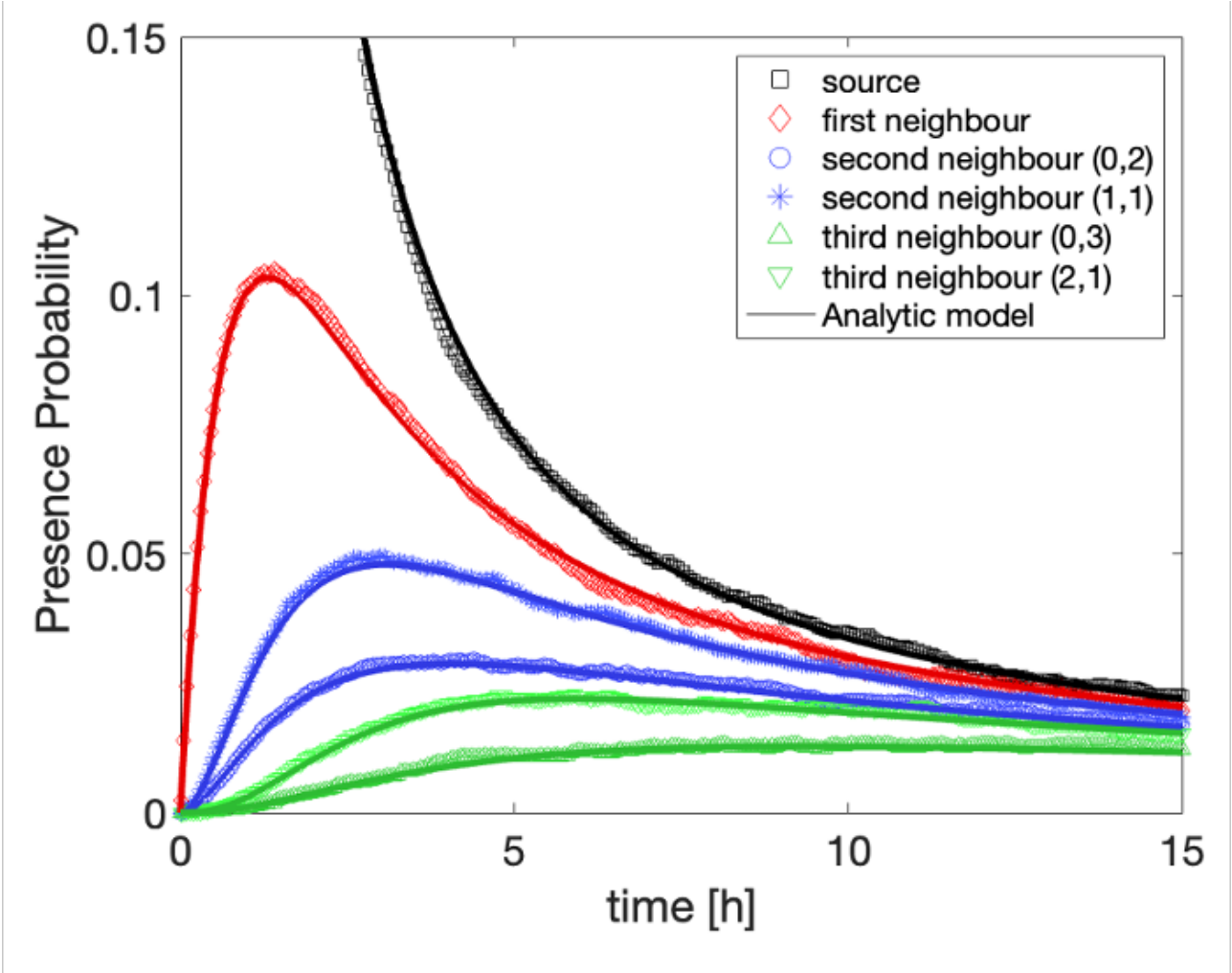

Figure S6: *Presence probability for a given position, obtained theoretically from Equation 23 (lines) and from simulations of a continuous-time random walk with exponential waiting times on a square lattice (symbols). Here, $\lambda = 1h^{-1}$ was chosen. The source is shown in black; first, second, and third neighbors are shown in red, blue, and green, respectively.*

main text). Consequently, in the following we will use the hexagonal theoretical model to analyze the experimental results.

Taylor expansion at short times

Taylor expansions of Equation 24 can be performed by taking $\lambda t \ll 1$. These fits allow us to extract values of λ, which were compared with those obtained experimentally. To extract the λ, we use the Taylor expansions of Equation 24. Thus, a first-order Taylor expansion can be performed for the first neighbor.

$$p((1,0),t) = \frac{e^{-\lambda_0 t}}{4\pi^2} \int_{-\pi}^{+\pi} \int_{-\pi}^{+\pi} dk_1 dk_2 \; cos(k_1) \; e^{\frac{\lambda_0 t}{3}(cos(k_1)+cos(k_2)+cos(k_1+k_2))}$$

Since $\lambda_0 t = \epsilon << 1$, thus, e^{ϵ} is approximated as $e^{\epsilon} \approx 1 + \epsilon$

$$p((1,0),t) = \frac{1-\epsilon}{4\pi^2} \int_{-\pi}^{+\pi} \int_{-\pi}^{+\pi} dk_1 dk_2 \; cos(k_1) \; (1 + \frac{\epsilon}{3}(cos(k_1) + cos(k_2) + cos(k_1+k_2)))$$

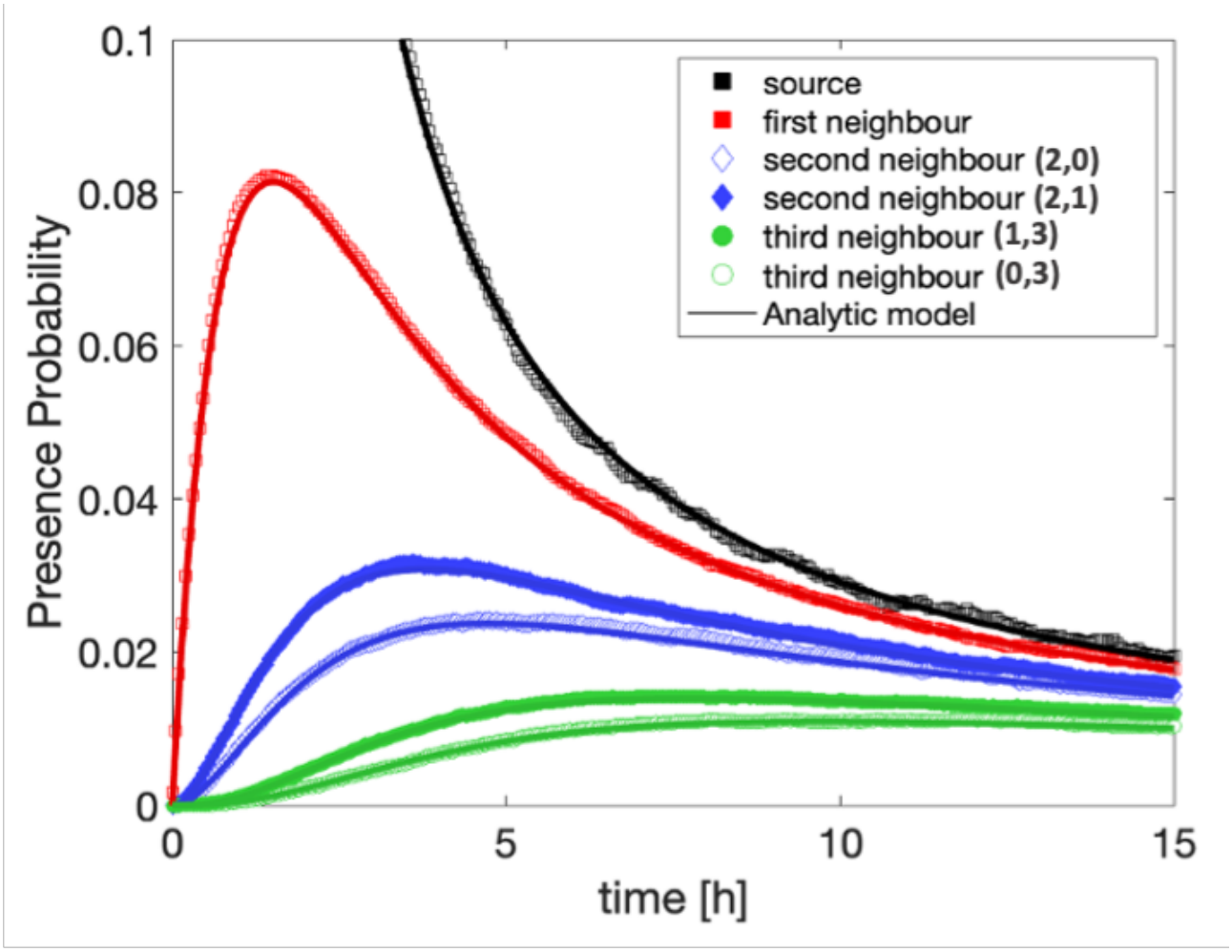

Figure S7: *Presence probability for a given position, obtained from Equation 24 (lines) and from simulations of a continuous-time random walk with exponential waiting times on a hexagonal lattice (symbols). $\lambda = 1h^{-1}$. The source is shown in black; first, second, and third neighbors are shown in red, blue, and green, respectively.*

$$p((1,0),t) = \frac{1-\epsilon}{4\pi^2}\Bigg[\underbrace{\int_{-\pi}^{+\pi}\int_{-\pi}^{+\pi} dk_1 dk_2\, \cos(k_1)}_{=0} + \underbrace{\int_{-\pi}^{+\pi}\int_{-\pi}^{+\pi} dk_1 dk_2\, \frac{\epsilon}{3}\cos(k_1)\Big(\cos(k_1)+\cos(k_2)+\cos(k_1+k_2)\Big)}_{=2\pi^2\times\frac{\epsilon}{3}}\Bigg]$$

Finally:

$$p((1,0),t) = \frac{1-\epsilon}{4\pi^2}\times 2\pi^2 \times \frac{\epsilon}{3} = \frac{(1-\epsilon)\epsilon}{6} = \frac{\epsilon}{6}$$

$$\boxed{p((1,0),t) = \frac{\lambda_0 t}{6}}$$

This result is intuitive: at the characteristic time $t = \frac{1}{\lambda_0}$, the walker has a probability of 1/6 of being at each first neighbor.

Similarly, for other neighbors the results of these expansions, for different sites and neighborhood degrees, are summarized in Table 1.

Neighborhood degree	**Site**	**Taylor expansion**
First neighbor	all	$\frac{\lambda_0 t}{6}$ At first order
Second neighbor	1 precursor	$\frac{(\lambda_0 t)^2}{72}$ At second order
Second neighbor	2 precursors	$\frac{(\lambda_0 t)^2}{36}$ At second order
Third neighbor	1 precursor	$\frac{(\lambda_0 t)^3}{1296}$ At third order
Third neighbor	2 precursors	$\frac{(\lambda_0 t)^3}{432}$ At third order

Table 1: Taylor expansions of presence probabilities for different neighborhood degrees and sites.

Heptamerization/Pentamerization Coupled Chemical Reactions

We investigate in this section how concomittent heptamerization/pentamerization oligomerization reactions can change the dependence of nanopores (αHL heptamers) with the concentration of monomer.

We consider two coupled chemical reactions, with respective reaction constant K_1 and K_2:

$$7M \xrightarrow{K_1} H,$$
$$5M \xrightarrow{K_2} P.$$

where M stands for 'Monomer', H for 'Heptamer' and P for pentamer.

Let $m(t) = [M](t)$, $h(t) = [H](t)$, and $p(t) = [P](t)$. The kinetic equations are:

$$\frac{dm}{dt} = -7K_1 m^7 - 5K_2 m^5,$$
$$\frac{dh}{dt} = K_1 m^7,$$
$$\frac{dp}{dt} = K_2 m^5.$$

Dividing the two first equations, one gets:

$$\frac{dh}{dm} = \frac{\frac{dh}{dt}}{\frac{dm}{dt}} = \frac{K_1 m^7}{-7K_1 m^7 - 5K_2 m^5} = -\frac{K_1 m^2}{7K_1 m^2 + 5K_2}.$$

If $(K_1/K_2)m$ is small, we have in a first approximation:

$$\frac{dh}{dm} \approx -\frac{K_1}{5K_2} m^2 \left(1 - \frac{7K_1}{5K_2} m^2 + O(m^4)\right).$$

Integrating, we obtain:

$$h(m) - h(m_0) \approx -\frac{K_1}{5K_2}\int_{m_0}^{m}\left(s^2 - \frac{7K_1}{5K_2}s^4\right)ds$$
$$= -\frac{K_1}{5K_2}\left[\frac{s^3}{3} - \frac{7K_1}{25K_2}s^5\right]_{m_0}^{m}.$$

Assuming $h(m_0) = 0$ and expanding for small m:

$$h(m) \approx -\frac{K_1}{15K_2}m^3 + \frac{7K_1^2}{125K_2^2}m^5 + O(m^7).$$

Thus, the concentration of the Heptamer is proportional to m^3 at low monomer concentration, with a correction term in m^5.

Supplementary Movies

Movie S1. Printing of aqueous droplets in an oil/lipid phase.
The movie shows the microfluidic deposition of water droplets into an oil phase supplemented with lipids, leading to the formation of stable droplet networks (time in seconds). The total duration of the movie is 5.22 seconds.

Movie S2. Compaction of droplets upon tilting to form a 2D network of droplet interface bilayers (DIBs).
The movie shows how aqueous droplets, initially dispersed in a lipid-containing oil phase, compact under gentle tilting of the chamber (time in minutes). This process drives the formation of a stable, compact two-dimensional network of DIBs. The total duration of the movie is 7 min 40 s.

Data availability

The data used in the paper can be downloaded from Zenodo folders (see the DAS file). The different experiment parameters are listed in the Table below :

Name of Experiment	$c_m[\mu\mathbf{g/mL}]$
24-07-01	75
24-07-02	50
24-07-03	125
24-07-04	100
24-07-16	150
24-08-20	75
24-08-22	0
24-08-26	125
24-08-27	100
24-08-28	150
24-09-09	125
24-09-10	100
24-09-16	150
24-10-07	50
24-10-09	100
24-10-14	150

Table 2: List of experiments used in the manuscript